THE JOURNAL OF BIOLOGICAL CHEMISTRY VOL. 288, NO. 45, pp. 32149–32159, November 8, 2013

Redox Control of the Senescence Regulator Interleukin-1α and the Secretory Phenotype*

Received for publication, June 19, 2013, and in revised form, September 11, 2013 Published, JBC Papers in Press, September 23, 2013, DOI 10.1074/jbc.M113.493841

Donald A. McCarthy, Ryan R. Clark, Toni R. Bartling, Mohamed Trebak, and J. Andres Melendez[1]

From the College of Nanoscale Science and Engineering, State University of New York, Albany, New York 12203

Background: The senescent microenvironment is permissive to disease progression, and the role of oxidants in this process remains uncharacterized.
Results: Senescent fibroblasts promote tumor invasion through redox/calcium regulation of the cytokine IL-1α.
Conclusion: Senescence-associated oxidants and calcium drive the secretory phenotype, altering the microenvironment.
Significance: Targeting senescent cells with antioxidant-based therapeutics may restrict inflammation and combat age-related disease progression.

Senescent cells accumulate in aged tissue and are causally linked to age-associated tissue degeneration. These non-dividing, metabolically active cells are highly secretory and alter tissue homeostasis, creating an environment conducive to metastatic disease progression. IL-1α is a key senescence-associated (SA) proinflammatory cytokine that acts as a critical upstream regulator of the SA secretory phenotype (SASP). We established that SA shifts in steady-state H_2O_2 and intracellular Ca^{2+} levels caused an increase in IL-1α expression and processing. The increase in intracellular Ca^{2+} promoted calpain activation and increased the proteolytic cleavage of IL-1α. Antioxidants and low oxygen tension prevented SA IL-1α expression and restricted expression of SASP components IL-6 and IL-8. Ca^{2+} chelation or calpain inhibition prevented SA processing of IL-1α and its ability to induce downstream cytokine expression. Conditioned medium from senescent cells treated with antioxidants or Ca^{2+} chelators or cultured in low oxygen markedly reduced the invasive capacity of proximal metastatic cancer cells. In this paracrine fashion, senescent cells promoted invasion by inducing an epithelial-mesenchymal transition, actin reorganization, and cellular polarization of neighboring cancer cells. Collectively, these findings demonstrate how SA alterations in the redox state and Ca^{2+} homeostasis modulate the inflammatory phenotype through the regulation of the SASP initiator IL-1α, creating a microenvironment permissive to tumor invasion.

Cellular senescence is an important tumor-constraining mechanism that halts cellular proliferation in response to damage that occurs during replication. However, senescent cells accumulate with age (1) and adopt a secretory phenotype that is causally linked to tissue degeneration (2). The senescence-associated (SA)[2] secretory phenotype (SASP) is regulated in large part by high level expression of IL-1α (3–6). Suppression of IL-1α expression or its biological function can extend cellular life span and restrict SA gene expression, but the mechanism of this age-dependent induction is unknown.

IL-1α is synthesized as a precursor protein that is subsequently cleaved into two functional fragments by the Ca^{2+}-activated protease calpain (7). The resulting C-terminal fragment of IL-1α (mature IL-1α) can bind IL-1 receptor I at the cell surface. IL-1 receptor I ligation elicits the production of inflammatory mediators, including IL-6 and IL-8 (6). The N-terminal propiece of IL-1α has a canonical nuclear localization sequence and can translocate into the nucleus. Once in the nucleus, the IL-1α propiece has been shown to act as a nuclear oncoprotein (8) and to promote the transcription of inflammatory genes (4, 9). These findings imply that IL-1α precursor processing may be required for full function and suggest that the regulated expression and subsequent processing of IL-1α are of functional significance. Recent evidence in immune cells supports this possibility, demonstrating that the processed form of IL-1α is more effective in inducing the production of inflammatory mediators (10).

Our findings indicate that SA IL-1α expression is induced by endogenous increases in intracellular H_2O_2. SA increases in intracellular Ca^{2+} levels provide sufficient quantities of this required cofactor for calpain activation. Consequently, calpain is aberrantly active in senescent cells and results in enhanced IL-1α processing. Reducing SA oxidative stress restricts inflammatory gene expression and effectively prevents senescent cells from adopting the SASP. Chelating Ca^{2+} during senescence inhibits calpain activation and IL-1α processing and attenuates the SASP phenotype. Functionally, restricting SA oxidative stress or aberrant Ca^{2+} signaling prevents senescent fibroblasts from promoting an invasive phenotype in proximal metastatic cancer epithelial cells. Together, these findings demonstrate how oxidant accumulation and Ca^{2+} deregulation during senescence coordinately influence the SASP and its impact on the tumor microenvironment.

EXPERIMENTAL PROCEDURES

Reagents—Calpain inhibitor (MDL28170; catalog no. 208719) was purchased from Calbiochem. *N*-Acetyl-L-cysteine (catalog no.

* This work was supported, in whole or in part, by National Institutes of Health Grant NIH R01 AG031067 (to J. A. M.).

[1] To whom correspondence should be addressed: College of Nanoscale Science and Engineering, State University of New York, 257 Fuller Rd., Albany, NY 12203. E-mail: jmelendez@albany.edu.

[2] The abbreviations used are: SA, senescence-associated; SASP, SA secretory phenotype; BAPTA-AM, 1,2-bis(2-aminophenoxy)ethane-*N*,*N*,*N*′,*N*′-tetraacetic acid tetrakis(acetoxymethyl ester); H_2DCFDA, 2′,7′-dichlorodihydrofluorescein diacetate; CDCF, 5(6)-carboxy-2′,7′-dichlorofluorescein diacetate; p, passage; CM, conditioned medium; SS-[H_2O_2], steady-state H_2O_2 concentration; EMT, epithelial-mesenchymal transition; qRT-PCR, quantitative real-time PCR.

A7250), recombinant catalase (catalog no. C40), and BAPTA-AM (catalog no. A1076) were purchased from Sigma-Aldrich. Wnt/β-catenin inhibitor ICG-001 (catalog no. S2662) was purchased from Selleck Chemical. Anti-N-terminal IL-1α (amino acids 2–112) antibody (catalog no. AF4154) was purchased from R&D Systems. Anti-μ-calpain antibodies were purchased from Abcam. Inactive μ-calpain was determined using an anti-N-terminal end domain I antibody that is targeted to an epitope that is cleaved during activation (catalog no. ab28257, Abcam). Total μ-calpain was determined using an anti-C-terminal end domain IV antibody (catalog no. ab39170, Abcam). Anti-E-cadherin antibody was purchased from Santa Cruz Biotechnology. Anti-N-cadherin antibody (catalog no. 2019-1) was purchased from Epitomics. Neutralizing antibody to mature IL-1α (catalog no. MAB200) was purchased from R&D Systems. Neutralizing antibody to IL-8 (catalog no. 554726) was purchased from Pharmingen. Neutralizing antibody to IL-6 (catalog no. P620) was purchased from Thermo Scientific.

Cell Culture—MDA-MB-231 and A549 cells were cultured in DMEM supplemented with 10% FBS. IMR-90 primary human fetal lung fibroblasts were cultured in minimal essential medium with 10% FBS and incubated at 21 or 3% oxygen tension at 37 °C with 5% CO_2. These cells were lifted in 0.05% trypsin/EDTA and serially passaged at a dilution of 1:4. Cells were transfected using FuGENE HD transfection reagent at a ratio of 2.5:1 reagent to plasmid DNA.

2′,7′-Dichlorodihydrofluorescein Diacetate (H_2DCFDA) Staining and ImageStreamX Analysis—The cell-permeant oxidation-sensitive dye H_2DCFDA (Invitrogen) was loaded into cells according to the manufacturer's protocol, followed by analysis by imaging flow cytometry. The oxidation-insensitive dye 5(6)-carboxy-2′,7′-dichlorofluorescein diacetate (CDCF; Invitrogen) was used as a control so that any changes in fluorescence seen between groups with the oxidation-sensitive dye could be directly attributed to changes in dye oxidation. Briefly, cells were loaded with 1 μM H_2DCFDA or CDCF in PBS for 45 min, followed by several PBS washes. The fluorescence intensity of oxidized DCF was measured using an Amnis ImageStreamX flow cytometer. The IDEAS software program was used to determine the mean fluorescence intensity and standard deviation for each sample. Mean fluorescent values for H_2DCFDA-treated cells were normalized to values for control CDCF-treated passage (p) 15 and p25 cells.

Real-time PCR—RNA was isolated from samples using TRIzol (Invitrogen) following the manufacturer's instructions. cDNA was synthesized using SuperScript III (Invitrogen) with random hexamers. Real-time PCR was performed with an Applied Biosystems 7500 real-time thermocycler with SYBR Green. Specific primers were used for each target, and the PCR conditions were as follows: 95 °C for 10 min, followed by 40 cycles of melting at 95 °C for 15 s, and annealing and elongation at 60 °C for 1 min. Product specificity was verified with a melt curve.

Immunofluorescence Microscopy—For filamentous actin staining, cells were fixed in an appropriate volume of methanol-free 4% formaldehyde diluted in PBS. These cells were then stained with Alexa Fluor 488-phalloidin conjugate (Invitrogen) according to the manufacturer's protocol. Cells expressing a DsRed-IL-1α N-terminal fusion construct were seeded on glass coverslips 1 day prior to imaging. The next day, these cells were washed three times with 1× PBS and fixed in an appropriate volume of 3 parts acetone to 2 parts PBS. Cells were imaged using an Olympus FV1000 confocal microscope. Nuclei were stained with DAPI that was present in the Prolong mounting medium (Invitrogen).

Senescence-associated β-Galactosidase Assay—Cells were stained for β-galactosidase (catalog no. 98603, Cell Signaling) at pH 6 following the manufacturer's instructions. Briefly, cells were fixed and stained overnight in a dry incubator at 37 °C. Staining was detected the following day using a light microscope. Cells positive for staining turned blue.

Calcium Imaging—Intracellular calcium levels were determined using ratiometric analysis of the calcium-binding dye Fura-2-AM (Invitrogen). This cell-permeable dye excites at 340 nm when bound to calcium and at 380 nm when unbound. Fluorescence intensities were then measured at an emission wavelength of 510 nm. These intensities were represented as a ratio of 340 to 380 nm.

Western Blot Analysis—Cells were lysed in an appropriate volume of radioimmune precipitation assay buffer (50 mM Tris-HCl, 150 mM NaCl, 1% Triton X-100, 1% sodium deoxycholate, 0.1% SDS, 0.1 mM Na_3VO_4, and protease inhibitors) at pH 7.5 for 15 min, with rotation at 4 °C. Cell debris was pelleted by centrifugation at 14,000 rpm at 4 °C, and the protein-containing supernatant was analyzed for protein concentration using BCA (Thermo Scientific). Equal amounts of protein were then subjected to PAGE and subsequently transferred to nitrocellulose membranes, followed by overnight incubation with primary antibodies at 4 °C. Blots were visualized using chemiluminescence. Where exogenous catalase uptake was measured, the cells were vigorously washed three times prior to cellular lysis to exclude any catalase that may have been attached to the cell surface.

Calpain Activity Assay—Calpain activity was measured using a calpain activity assay kit (catalog no. K240-100, BioVision). Briefly, 1×10^6 cells were pelleted by centrifugation, followed by resuspension in extraction buffer on ice for 20 min. Equal amounts of lysate (normalized to total protein) were incubated with fluorescently labeled calpain substrate at 37 °C for 1 h. Relative fluorescence was measured in a plate reader with a 400-nm excitation filter and 505-nm emission filter.

Matrigel Invasion Assay—24-well chamber inserts precoated with Matrigel (BD Biosciences) were partly submerged in 750 μl of conditioned medium (CM) collected over 18 h. MDA-MB-231 cells were placed in the top chamber in serum-free medium and allowed to invade over 22 h. Non-invading cells were removed from the insert with cotton-tipped applicators. Invaded cells were fixed in 100% methanol for 20 min at −20 °C and mounted on Prolong mounting medium containing DAPI for visualization.

Primers for Real-time PCR—The primers used were as follow: IL-1α, AACCAGTGCTGCTGAAGGA (sense) and TTCTTAGTGCCGTGAGTTTCC (antisense); actin, ACCAACTGGGACGACATGGAGAAA (sense) and TAGCACAGCCTGGATAGCAACGTA (antisense); IL-6, CCACACAGACAGCCACTCACC IL-6 (sense) and CTACATTTGCCGAAGAGCCCTC (antisense); and IL-8, CTCTCTTGGCAGCCTTCCTGATT (sense) and AACTTCTCCACAACCCTCTGCAC (antisense).

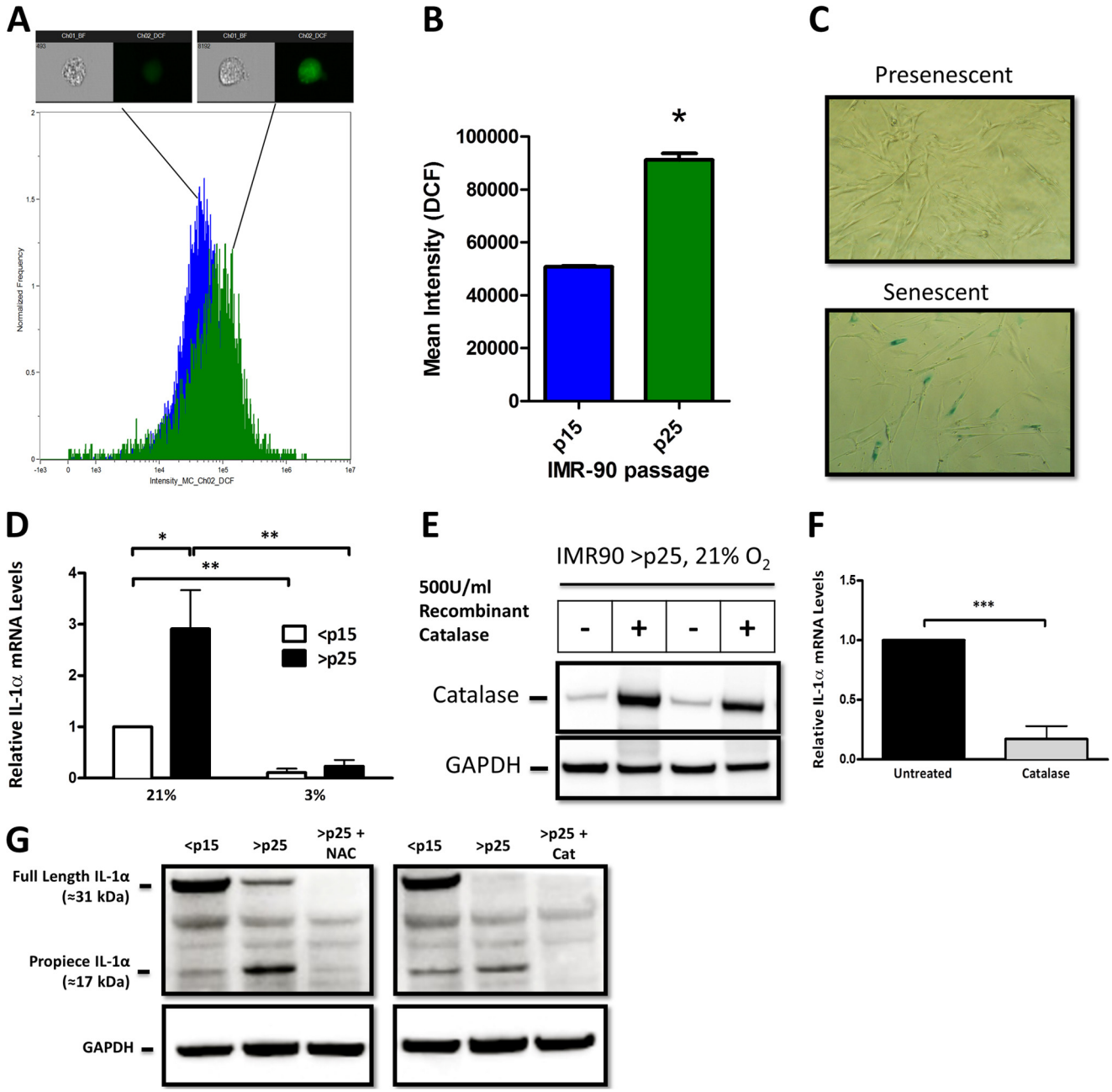

FIGURE 1. **SA IL-1α expression is regulated by cellular H_2O_2.** *A*, histogram of data obtained using an ImageStreamX flow cytometer to investigate the fluorescence intensity of the reactive oxygen species-sensitive dye H_2DCFDA in IMR-90 cells. Presenescent (<p15; $n = 8070$) and senescent (>p25; $n = 3458$) cells were quantified for DCF intensity. One representative image is shown from the bin corresponding to the mean intensity of the 505–560-nm emission channel for each population. Positive DCF staining is shown in *green* in the cell image inlay. Mean fluorescent values for cells treated with H_2DCFDA were normalized to control DCF-treated values for <p15 and >p25 cells. *B*, bar graph of the ImageStreamX data. The IDEAS software program was used to calculate the mean intensity of the DCF signal for each sample, and the results are plotted with *error bars* that represent S.D. *C*, SA β-galactosidase staining in presenescent (<p15) and senescent (>p25) IMR-90 fibroblasts cultured in 21% O_2. *D*, quantitative real-time PCR (qRT-PCR) of the IL-1α transcript from presenescent (<p15) and senescent (>p25) IMR-90 fibroblasts cultured in 21 or 3% O_2. *E*, Western blot analysis of intracellular catalase after overnight incubation with 500 units/ml recombinant catalase added to cell culture medium. GAPDH was used as a loading control. *F*, qRT-PCR of the IL-1α transcript from senescent cells with and without 500 units/ml recombinant catalase. *G*, Western blot analysis of IL-1α protein using an antibody directed against an N-terminal epitope (amino acids 2–112) in <p15 and >p25 cells. *N*-Acetyl-L-cysteine (*NAC*) was used at a concentration of 2 mM, and recombinant catalase (*Cat*) was used at 500 units/ml. Data represent $n \geq 3$. *, $p \leq 0.05$; **, $p \leq 0.01$; ***, $p \leq 0.001$.

RESULTS

Senescence-associated IL-1α Expression Is Regulated by Cellular H_2O_2—IL-1α expression increases as cells near their replicative life span (3–6), and this elevated expression coincides with an increase in oxidation of the redox-sensitive fluorophore H_2DCFDA (Fig. 1, *A* and *B*) and supports prior work indicating that senescence is accompanied by increases in steady-state H_2O_2 concentration (SS-[H_2O_2]) (11). Because SA increases in IL-1α and SS-[H_2O_2] occur concurrently, we first determined if shifts in SS-[H_2O_2] influence the expression of SA IL-1α. Primary human fibroblasts (IMR-90) approach their replicative life span in 21% O_2 at or near 50 population doublings (≈p25),

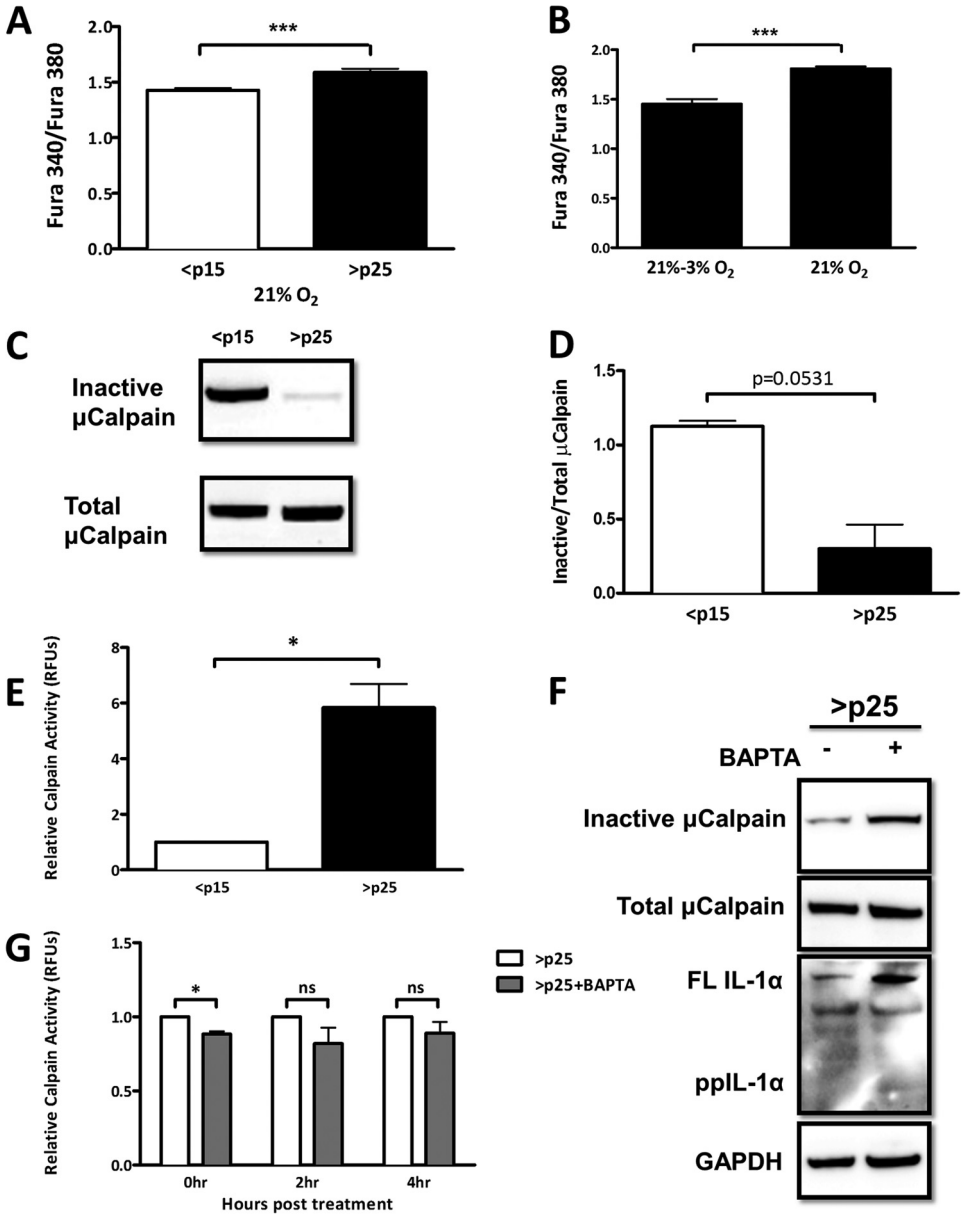

FIGURE 2. **SA shifts in intracellular Ca^{2+} activate calpain and promote IL-1α processing.** *A*, ratiometric Ca^{2+} imaging of presenescent (<p15) and senescent (>p25) primary IMR-90 fibroblasts. *B*, ratiometric Ca^{2+} imaging of senescent (>p25) IMR-90 fibroblasts maintained at 21% oxygen tension or moved to 3% oxygen tension. Cells were assayed 1 week after changing the oxygen tension. *C*, Western blot analysis of inactive and total μ-calpain in presenescent and senescent cells. *D*, quantification of *C*. *E*, calpain activity measured using fluorescently labeled substrate in presenescent (<p15) and senescent (>p25) primary IMR-90 fibroblasts. *RFU*, relative fluorescence units. *F*, Western blot analysis of inactive and total μ-calpain and IL-1α in senescent cells 6 h post-treatment with and without 3 μM BAPTA-AM (pulsed for 1 h). *FL IL-1α*, full-length IL-1α; *ppIL-1α*, IL-1α propiece. *G*, calpain activity measured using fluorescently labeled substrates in senescent cells with and without 3 μM BAPTA-AM (pulsed for 1 h) at the indicated times post-treatment. Data represent $n \geq 3$. *, $p \leq 0.05$; ***, $p \leq 0.001$; *ns*, not significant.

which coincides with increased SS-[H_2O_2] (11) and SA β-galactosidase activity (Fig. 1*C*). Maintaining cells in a low (3%) O_2 environment reduces SS-[H_2O_2] and oxidative damage and delays the onset of senescence (11–13). IL-1α expression was increased in senescent (>p25) cells cultured in 21% O_2, but not in the replicative age-matched controls cultured in 3% O_2 (Fig. 1*D*). To further define the oxidant dependence of this process, late passage (>p25) cells were treated with recombinant catalase, and IL-1α levels were determined. When added to the medium, catalase gains entry into cells, where it specifically scavenges H_2O_2 (14). Exogenous catalase loading was confirmed (Fig. 1*E*) and significantly reduced IL-1α expression in >p25 cells (Fig. 1*F*). In addition, treatment with catalase or the glutathione precursor *N*-acetyl-L-cysteine abrogated SA IL-1α expression in late passage cells (Fig. 1*G*). Notably, production of SA IL-1α was accompanied by preferential processing to its 17-kDa form (Fig. 1*G*). Together, these data indicate that shifts in oxidant production control SA increases in IL-1α expression and processing.

Senescence-associated Shifts in Intracellular Ca^{2+} Activate Calpain and Promote IL-1α Processing—Calpain, a protease that processes IL-1α, is functionally dependent on the availability of Ca^{2+}, the homoeostasis of which can be oxidant-sensitive (15–17). To determine whether senescent cells display altera-

tions in $[Ca^{2+}]_i$, we used the cell-permeant Ca^{2+}-binding ratiometric fluorophore Fura-2-AM and monitored $[Ca^{2+}]_i$ in both <p15 and >p25 cells. Senescent cells displayed higher basal $[Ca^{2+}]_i$ than presenescent cells (Fig. 2*A*), which was attenuated in cells acutely exposed to low oxygen (3%) (Fig. 2*B*). Ca^{2+} is a required cofactor for calpain activity; thus, we next determined the degree of calpain activation in <p15 and >p25 cells. Upon Ca^{2+}-dependent activation, calpain undergoes autolysis, which involves the removal of several N-terminal residues (18). Utilizing antibodies that recognize either the N-terminal epitope that is lost upon activation or total calpain, we determined the degree of calpain activation by immunoblotting. Total calpain levels were similar between <p15 and >p25 cells; however, the amount of inactive calpain was decreased in >p25 cells (Fig. 2, *C* and *D*), suggesting that calpain in these cells is primarily in its active state. We next measured calpain activity in <p15 and >p25 cells using fluorescently tagged substrates. This assay quantitatively confirmed our findings, displaying an ~6-fold increase in calpain activity during senescence (Fig. 2*E*). To link SA increase in $[Ca^{2+}]_i$ to calpain activation, we next treated >p25 cells with BAPTA-AM, a Ca^{2+}-specific chelator, and measured calpain activation quantitatively and by immunoblotting. Ca^{2+} chelation restricted calpain activity, albeit in a modest and short-lived fashion (Fig. 2, *F* and *G*). Furthermore, SA IL-1α processing was effectively prevented when >p25 cells were treated with BAPTA-AM (Fig. 2*F*). Together, these data identify SA shifts in Ca^{2+} homeostasis that are linked to aberrant calpain activation and IL-1α processing.

SA IL-1α Is Localized to the Nucleus in a Redox- and Calpain-dependent Fashion—IL-1α processing is often accompanied by its cellular redistribution (9, 19). To determine IL-1α localization, <p15 and >p25 IMR-90 cells were transiently transfected with a DsRed-IL-1α N-terminal fusion construct, and its cellular distribution was monitored when exposed to low or ambient O_2 tension. DsRed-IL-1α was localized primarily in the nucleus in >p25 cells, but not in <p15 cells cultured in 21% O_2 (Fig. 3, *A* and *B*). Cells maintained at 3% O_2 abrogated the SA IL-1α nuclear localization compared with their age-matched controls maintained at 21% O_2 (Fig. 3*C*). Treatment with recombinant catalase prevented IL-1α nuclear localization (Fig. 3*D*), further implicating H_2O_2 in this process. Furthermore, SA IL-1α was excluded from the nucleus of cells treated with a calpain inhibitor (Fig. 3*E*), indicating calpain involvement. Together, these findings support a role for oxidants and calpain in SA IL-1α nuclear localization.

Oxidative Stress and Ca^{2+} Regulate the SASP—SA IL-1α has been reported to functionally act as an initiator of the SASP (1, 6, 20), which is characterized by high levels of inflammatory cytokines, such as IL-6 and IL-8. We confirmed, this finding using a neutralizing antibody against the secreted form of IL-1α (mature IL-1α), which inhibited the SA expression of both IL-6 and IL-8 (Fig. 4*A*). Interestingly, IL-1α neutralization also inhibited the expression of nascent IL-1α, suggesting a feed-forward mechanism (Fig. 4*A*). To investigate whether the SASP is also under redox control, we monitored SA IL-6 and IL-8 expression in cells exposed to 21 and 3% O_2 or treated with an antioxidant. Both IL-6 and IL-8 mRNA levels were increased during senescence, but only IL-6 (not IL-8) expression was attenuated by low oxygen tension (Fig. 4, *A* and *B*). However, SA expression of both cytokines was prevented by the addition of the H_2O_2-scavenging enzyme catalase (Fig. 4*C*). Treatment of senescent cells with BAPTA-AM also reduced the expression of IL-8, but not IL-6, at 5 and 7 h post-treatment (Fig. 4, *D* and *E*). IL-6 levels decreased modestly, but insignificantly ($p = 0.10$), at 7 h post-treatment. Later time points may be needed to determine whether the effect on IL-6 is delayed. Inhibition of the IL-1α-processing enzyme calpain caused a reduction in the expression of both IL-6 and IL-8 (Fig. 4*F*). Our findings further support a role for IL-1α as an upstream regulator of the SASP (6) and now implicate both redox and Ca^{2+}-dependent processes in its ability to regulate the prominent SASP factors IL-6 and IL-8.

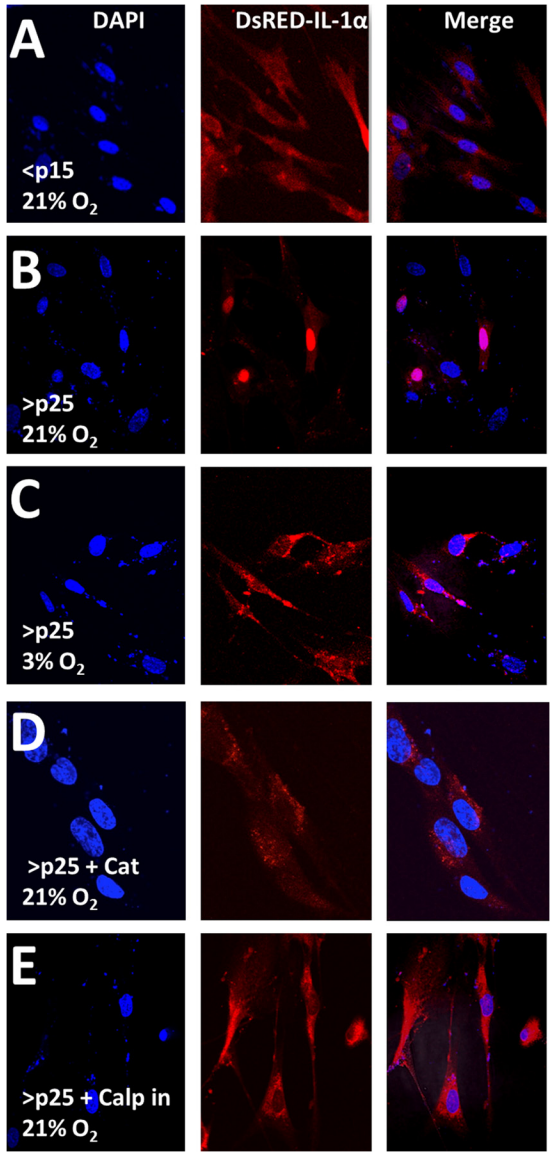

FIGURE 3. **SA IL-1α is localized to the nucleus in a redox- and calpain-dependent fashion.** *A–E*, confocal microscopy of a DsRed-IL-1α construct 16 h post-transient transfection into IMR-90 fibroblasts passaged as indicated at 21 or 3% O_2 tension. Catalase (*Cat*) was added exogenously at 500 units/ml 3 h post-transfection. The calpain inhibitor (*Calp*) was used at a concentration of 40 μM and was added to the medium 3 h post-transfection. Data represent $n \geq 3$.

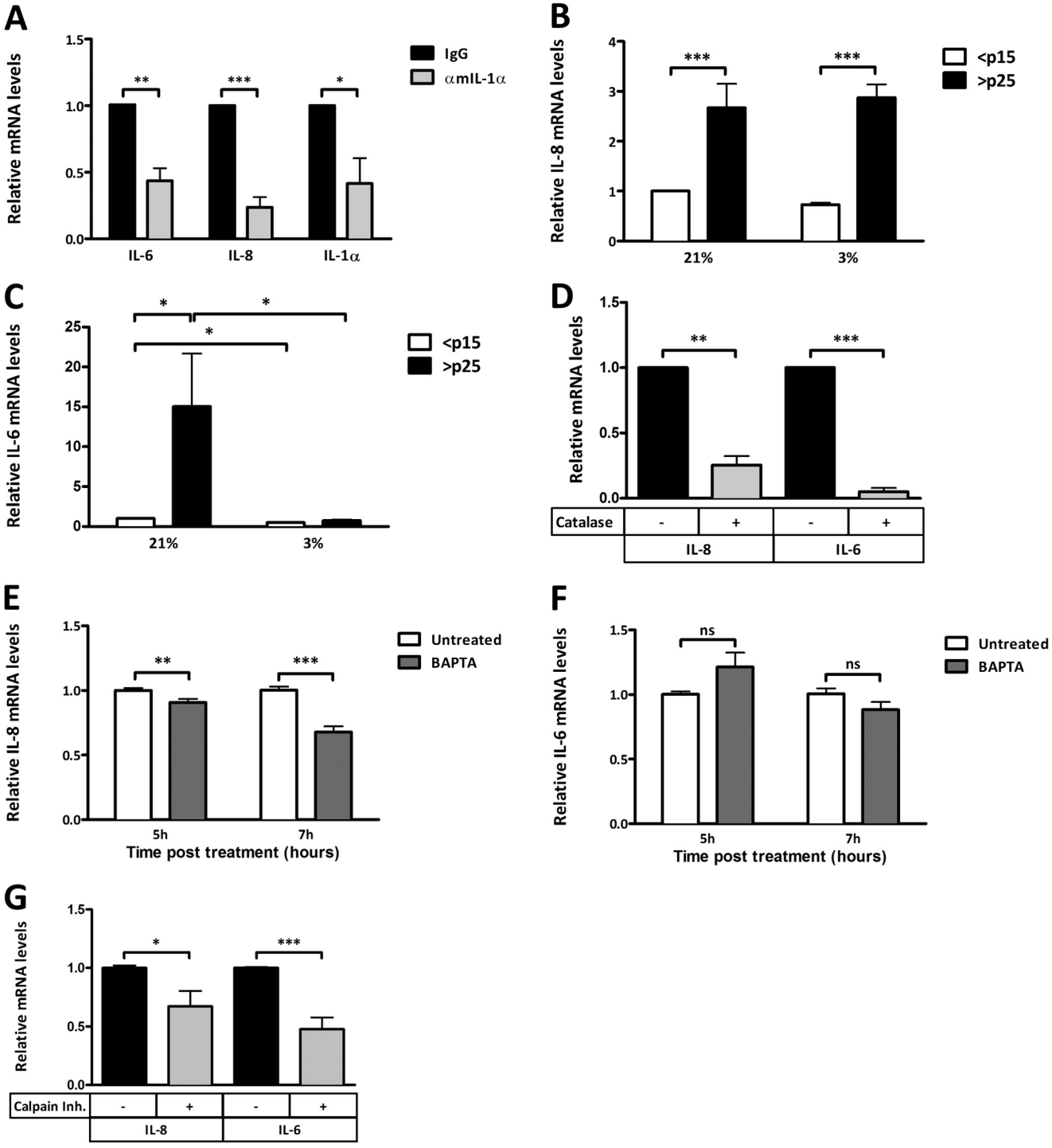

FIGURE 4. **Oxidative stress and Ca^{2+} regulate the SASP.** *A*, qRT-PCR of IL-6, IL-8, and IL-1α transcripts in senescent cells with or without neutralizing antibody to secreted mouse IL-1α (*αmIL-1α*). *B*, qRT-PCR of the IL-8 transcript from presenescent (<p15) and senescent (>p25) IMR-90 fibroblasts cultured in 21 or 3% O_2. *C*, qRT-PCR of the IL-6 transcript from presenescent (<p15) and senescent (>p25) IMR-90 fibroblasts cultured in 21 or 3% O_2. *D*, qRT-PCR of IL-6 and IL-8 transcripts from senescent IMR-90 fibroblasts with and without 500 units/ml recombinant catalase. *E*, qRT-PCR of the IL-8 transcript from senescent IMR-90 fibroblasts with and without 3 μM BAPTA-AM (pulsed for 1 h) at the indicated times post-treatment. *F*, qRT-PCR of the IL-6 transcript from senescent IMR-90 fibroblasts with and without 3 μM BAPTA-AM (pulsed for 1 h) at the indicated times post-treatment. *G*, qRT-PCR of IL-6 and IL-8 transcripts from senescent IMR-90 fibroblasts with and without 4 μM calpain inhibitor (*Inh.*) 18 h post-treatment. Data represent $n \geq 3$. *, $p \leq 0.05$; **, $p \leq 0.01$; ***, $p \leq 0.001$; *ns* not significant.

Limiting SA Oxidant Production or Intracellular Ca^{2+} Restricts SASP-mediated Tumor Cell Invasion—SASP factors can act on neighboring tissue, promoting the invasive properties of premalignant cells (1). We next tested whether the invasive behavior of metastatic breast cancer cells (MDA-MB-231) is sensitive to exposure to CM from IMR-90 fibroblasts cultured in 21 or 3% O_2 or treated with antioxidants. CM collected from cells exposed to 3% O_2 failed to induce significant Matrigel invasion compared with CM from cells exposed to 21% O_2. CM from <p15 cultures exposed to 21 or 3% O_2 had no impact

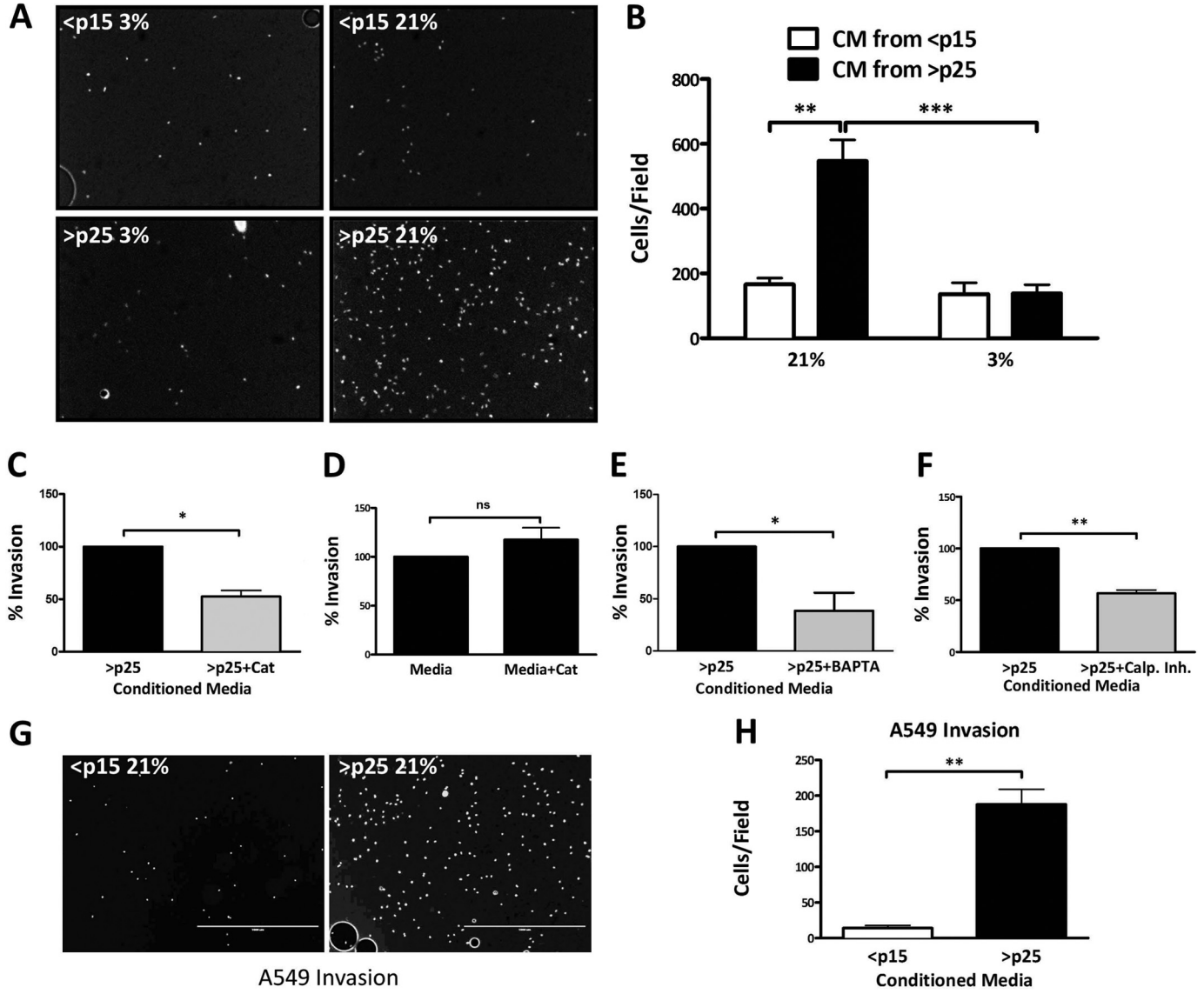

FIGURE 5. **Limiting SA oxidant production or intracellular Ca^{2+} restricts SASP-mediated tumor cell invasion.** *A*, representative images of invaded MDA-MB-231 breast cancer cells submerged in CM collected over 18 h from IMR-90 fibroblasts cultured and passaged as indicated. *B*, quantification of Matrigel invasion assay as described for *A*. Data represent $n \geq 3 \pm$ S.E. *C*, Matrigel invasion assay of MDA-MB-231 breast cancer cells submerged in CM from senescent IMR-90 fibroblasts with and without treatment with 500 units/ml catalase (*Cat*) prior to CM collection. *D*, Matrigel invasion assay of invaded MDA-MB-231 breast cancer cells in serum-containing medium collected over 18 h with and without the addition of 500 units/ml recombinant catalase. *E*, Matrigel invasion assay of MDA-MB-231 breast cancer cells submerged in CM from senescent IMR-90 fibroblasts with and without 3 μM BAPTA-AM (pulsed for 1 h). CM was collected 18 h post-treatment. *F*, Matrigel invasion assay of MDA-MB-231 breast cancer cells submerged in CM from senescent IMR-90 fibroblasts with and without 4 μM calpain inhibitor. CM was collected 18 h post-treatment. *G*, representative images of invaded A549 lung carcinoma cells submerged in CM collected over 18 h from IMR-90 fibroblasts passaged as indicated. *H*, quantification of Matrigel invasion assay as described for *G*. Data represent $n \geq 3$. *, $p \leq 0.05$; **, $p \leq 0.01$; ***, $p \leq 0.001$; *ns* not significant.

on the invasive capacity of MDA-MB-231 cells (Fig. 5, *A* and *B*). Similarly, senescent CM collected from cells treated with recombinant catalase significantly reduced the number of invading cells (Fig. 5*C*), whereas direct catalase exposure of the MDA-MB-231 cells had no impact on their invasive potential (Fig. 5*D*). Collectively, these data demonstrate that the ability of senescent CM to drive the invasive potential of proximal cancer cells is redox-sensitive. We next exposed >p25 cells to BAPTA-AM and a calpain inhibitor and monitored the ability of senescent CM to promote invasion. BAPTA-AM modestly but significantly impaired invasion driven by exposure to senescent CM, similar to its impact on IL-6 and IL-8 (Fig. 5*E*). Treatment of >p25 cells with a calpain inhibitor also significantly reduced the resultant invasion of breast cancer cells cultured in this CM (Fig. 5*F*). MD-MB-231 cells are highly invasive, and therefore, it was of interest to test the effects of CM on the less invasive A549 lung carcinoma cells. Much like the effect on MDA-MB-231 cells, CM from >p25 fibroblasts increased invasion relative to CM from <p15 fibroblasts (Fig. 5, *G* and *H*). Overall, these findings establish that SASP impairment in response to low oxygen, antioxidant treatment, Ca^{2+} chelation, or calpain inhibition can limit paracrine signaling that promotes neighboring tumor cell invasion.

Actin Remodeling in MDA-MB-231 Cells Is Driven by Exposure to Conditioned Medium from Senescent Cells—We next evaluated the distribution of filamentous actin in MDA-MB-

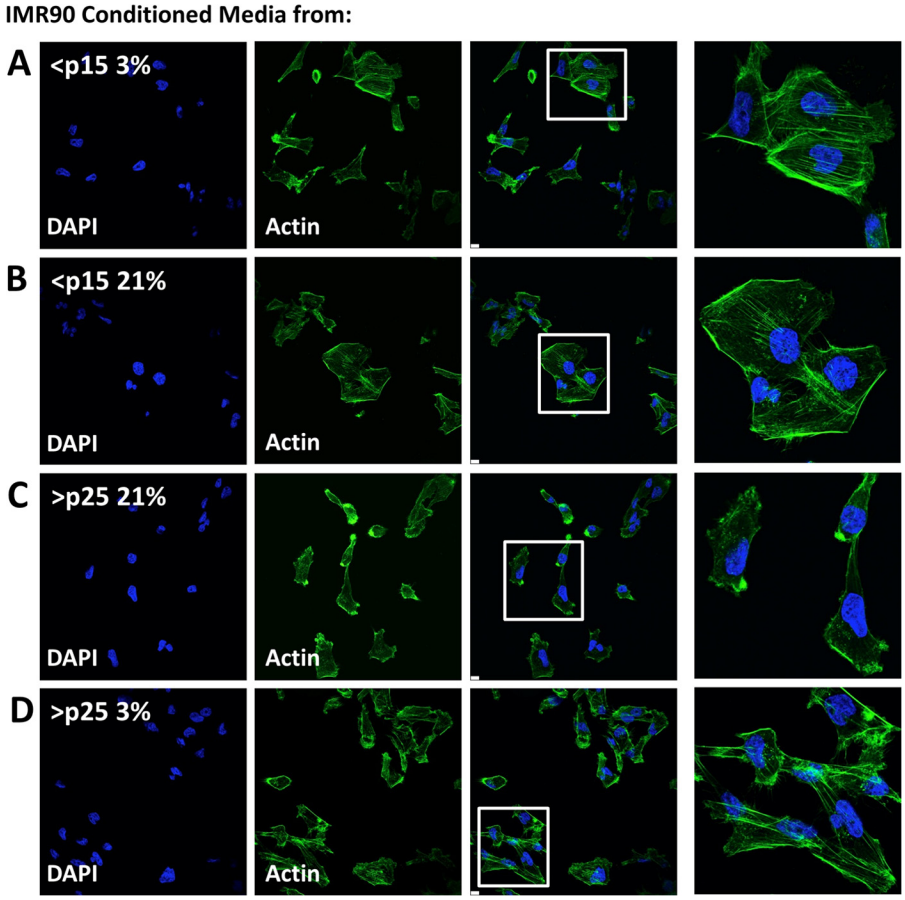

FIGURE 6. **Actin remodeling in MDA-MB-231 cells is driven by exposure to CM from senescent cells.** *A–D*, confocal microscopy of filamentous actin (stained with Alexa Fluor 488-phalloidin conjugate) in MDA-MB-231 breast cancer cells after incubation with CM from IMR-90 fibroblasts cultured to senescence at 21 or 3% O_2 tension. Nuclei were stained with DAPI. Data represent $n \geq 3$.

231 cells exposed to fibroblast CM, as actin reorganization and polarization are critical steps in the process of epithelial transformation (21, 22). MDA-MB-231 cells treated with CM from early and late passage cells cultured in low O_2 maintained actin stress fibers and a more cuboidal phenotype (Fig. 6, *A*, *B*, and *D*). MDA-MB-231 cells exposed to CM from late passage IMR-90 cells maintained in 21% O_2 displayed a distinct alteration in cellular polarity and loss of stress fibers, as shown in Fig. 6*C*. These data further support the notion that senescent fibroblasts promote proximal epithelial invasion and delineate a mechanism by which SASP-dependent transformation is responsive to shifts in oxygen tension.

Redox Control of SASP-mediated Tumor Cell Invasion and Transformation—The SASP factors IL-6 and IL-8 have been shown to promote epithelial-mesenchymal transition (EMT) (23, 24) that accompanies cancer cell invasion. This was confirmed by treating senescent CM with neutralizing antibodies to both IL-6 and IL-8 and monitoring tumor cell invasion (Fig. 7*A*). A hallmark of EMT is loss of expression of the tight junction component and epithelial marker E-cadherin (25). MDA-MB-231 cells incubated with senescent CM repressed E-cadherin expression in breast cancer cells compared with CM from <p15 fibroblasts (Fig. 7*B*). Canonical Wnt signaling is another hallmark of EMT and results in the accumulation of the mesenchymal marker β-catenin (26–28). Exposure of MDA-MB-231 cells to senescent CM increased β-catenin levels (Fig. 7*B*), demonstrating both a loss of an epithelial phenotype and acquisition of a more mesenchymal phenotype. However, the levels of the mesenchymal marker N-cadherin were unaffected by exposure to senescent CM (Fig. 7*B*), which is likely explained by the fact that MDA-MB-231 cells display unusually high basal expression of this protein (29). We next monitored EMT markers in A549 lung carcinoma cells exposed to CM from early and late passage cells. Similar to the breast cancer cells, A549 cells increased their expression of β-catenin when cultured with senescent CM (Fig. 7*C*). However, distinct from the breast cancer cells, A549 cells increased their levels of N-cadherin, whereas expression of E-cadherin was unaffected by exposure to senescent CM (Fig. 7*C*). Overall, the alterations in the levels of these mesenchymal markers suggest the engagement of an EMT process. The lack of effect on E-cadherin in the A549 cells may be explained by the recent observation that its localization rather than its expression can be altered during EMT (30).

Accumulation of β-catenin results in its translocation to the nucleus, where it acts as a coactivator of T cell factor/lymphoid enhancer factor-dependent transcription (31). Formation of this nuclear complex causes EMT and increases tumor invasiveness (32). To determine whether senescent CM promotes epithelial invasion through this pathway, tumor cells were treated with the β-catenin/T cell factor-specific transcriptional inhibitor ICG-001 (33), and invasion was monitored. Senescent CM-induced invasion in both cell lines was decreased by ICG-

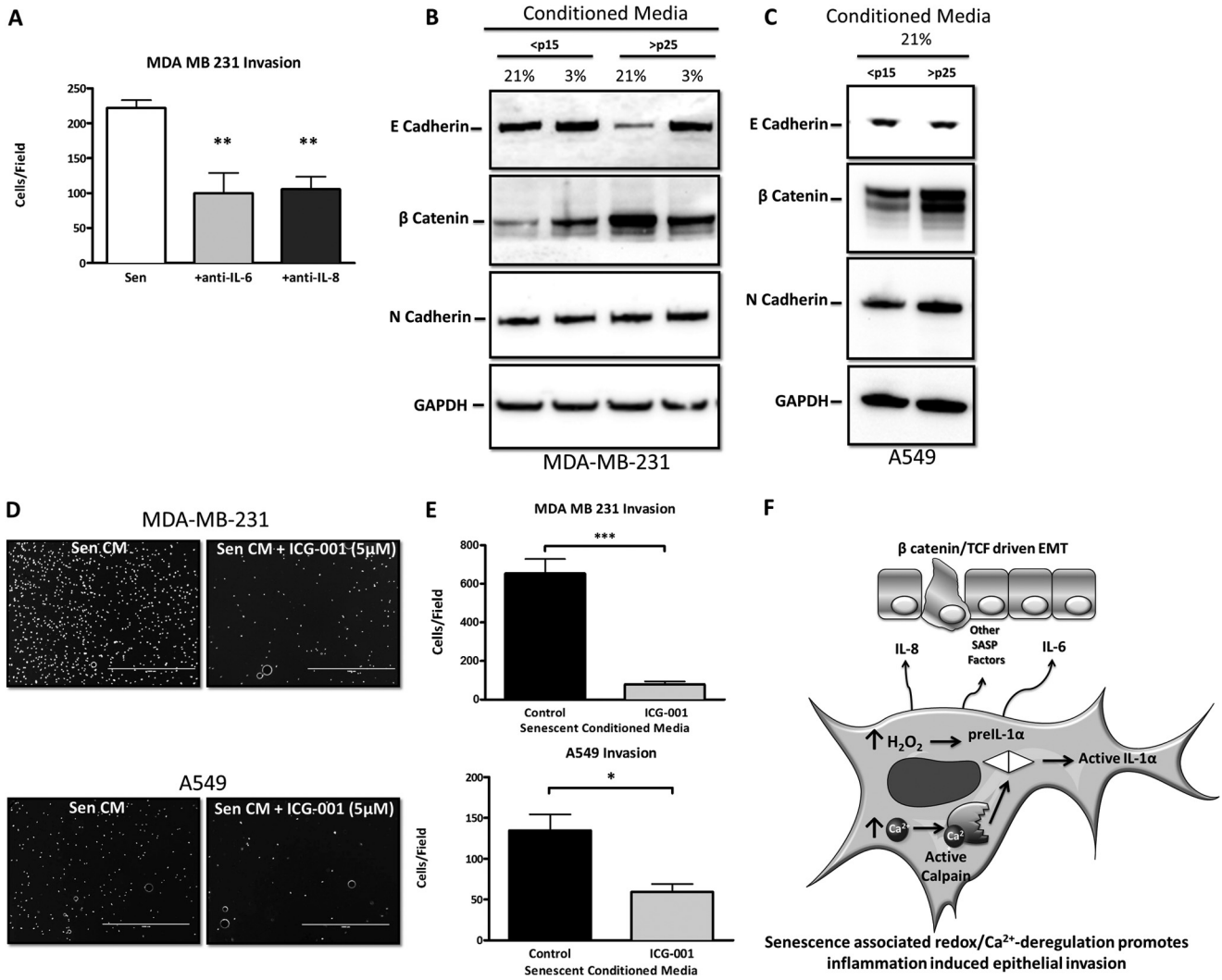

FIGURE 7. **Redox control of SASP-mediated tumor cell invasion and transformation.** *A*, Matrigel invasion assay of MDA-MB-231 breast cancer cells submerged in CM from senescent IMR-90 fibroblasts (*Sen*) with and without neutralizing antibody against IL-6 or IL-8. *B*, Western blot analysis of epithelial marker E-cadherin and mesenchymal markers β-catenin and N-cadherin in MDA-MB-231 cells cultured in IMR-90 CM. *C*, Western blot analysis of epithelial marker E-cadherin and mesenchymal markers β-catenin and N-cadherin in A549 cells cultured in IMR-90 CM. *D*, representative images of invaded MDA-MB-231 breast cancer cells and A549 lung carcinoma cells submerged in CM collected over 18 h from senescent IMR-90 fibroblasts with and without 5 μM ICG-001 added to CM immediately prior to use. *E*, quantification of *D*. *F*, model demonstrating how redox/Ca^{2+}-stressed senescent fibroblasts synergistically promote epithelial invasion in adjacent epithelial cells through their secretory phenotype. Data represent $n \geq 3 \pm$ S.E. *, $p \leq 0.05$; **, $p \leq 0.01$; ***, $p \leq 0.001$. *TCF*, T cell factor.

001 (Fig. 7, *D* and *E*). These findings suggest that senescent CM affects neighboring epithelial invasion and transformation through the β-catenin/T cell factor signaling complex (Fig. 7*F*). Our data are consistent with a report that came out during preparation of this manuscript describing the SASP as able to drive EMT in mesothelioma cells (34) and now demonstrate an oxidant-dependent regulation of SASP-driven EMT through β-catenin.

DISCUSSION

Here, we have provided evidence that the cellular redox state is an important parameter controlling the senescent phenotype. We established that increases in SS-[H_2O_2] (11) drive IL-1α expression during cellular senescence and may account for the increase in IL-1α levels in organismal models of senescence (3–6). We established that this redox-dependent increase in IL-1α expression occurs at the transcriptional level and can be modulated with the use of antioxidants. This is of functional significance, as IL-1α is an important upstream regulator of the SASP (6), providing a possible strategy to restrict other downstream components of the SASP. Indeed, we found that antioxidants can also restrict the SA levels of IL-6 and IL-8.

We have presented evidence that IL-1α processing is influenced by cellular life span and the accumulation of intracellular Ca^{2+}. Our findings establish that SA processing of precursor IL-1α involves the Ca^{2+}-dependent protease calpain. We believe that this differential processing event may be indirectly influenced by the redox environment of the cell, as alterations in redox state are often coupled to shifts in Ca^{2+} homeostasis. Future work will be directed at defining the precise redox triggers that drive shifts in SA calcium homeostasis. Altered Ca^{2+} flux leading to calpain-dependent processing of IL-1α has also been implicated in cells of hematopoietic origin in response to infection with *Listeria monocytogenes* (35) and when cation chan-

nels are forced open (36). These previous studies demonstrate that uncoupling the intracellular/extracellular Ca^{2+} gradient activates calpain and increases the processing and secretion of IL-1α. Our data add an additional element, showing that replicative aging initiates Ca^{2+} flux and promotes IL-1α processing.

The redox-dependent expression and subsequent processing of IL-1α provide a therapeutic avenue to limit the activity of this central regulator of SA inflammation. The feasibility of this approach was demonstrated using H_2O_2-specific antioxidants, showing they can dramatically reduce SA IL-1α expression and ultimately prevent expression of the downstream SASP factors IL-6 and IL-8. Interestingly, IL-8 expression is not sensitive to low O_2 exposure, which is likely explained by the fact that IL-8 expression can be regulated by hypoxia-inducible factor-1α (37–39), which is stabilized in the 0.1–4% O_2 range (40). Although antioxidants limit the expression of IL-1α, they may also prevent the Ca^{2+}-dependent processing of this factor. This may enhance the efficacy of this approach because processing seems to be required for full function of this cytokine. Indeed, IL-1α processing was found to enhance its biological activity and increase its ability to drive IL-6 and IL-8 expression (10). Our findings suggest that, as cells age, they enhance the processing of SA IL-1α, creating foci where the duration and amplitude of the inflammatory response may be dramatically enhanced either in an autocrine or a paracrine fashion by IL-1α itself.

It is hypothesized that SA increases in IL-1α expression and processing drive the SASP, creating a microenvironment that is conducive to metastatic disease progression. Our findings indicate that senescent cells can be rendered incapable of promoting neighboring cell invasion and transformation by modulating the redox state, Ca^{2+} levels, or the IL-1α-processing enzyme calpain. This age-related phenotype shift serves to propagate inflammation-associated disease and promote tumor invasion, with senescent cells serving as the seeding grounds for these processes (Fig. 7*F*). Although we have established that antioxidants can restrict the capacity of SASP-driven tumor cell invasion *in vitro*, recent work has established that ablation of senescent cells *in vivo* can limit age-associated cataracts and muscle loss (2). In this context, the SA redox environment becomes a very important therapeutic target for antioxidant-based treatment of age-associated degenerative disease.

Acknowledgments—We thank Dr. Guangming Zhong for generously providing the DsRed-IL-1α construct. Portions of this work were performed at the Center for Immunology and Microbial Disease of Albany Medical College (Albany, NY).

REFERENCES

1. Campisi, J. (2005) Senescent cells, tumor suppression, and organismal aging: good citizens, bad neighbors. *Cell* **120,** 513–522
2. Baker, D. J., Wijshake, T., Tchkonia, T., LeBrasseur, N. K., Childs, B. G., van de Sluis, B., Kirkland, J. L., and van Deursen, J. M. (2011) Clearance of $p16^{Ink4a}$-positive senescent cells delays ageing-associated disorders. *Nature* **479,** 232–236
3. Mariotti, M., Castiglioni, S., Bernardini, D., and Maier, J. A. (2006) Interleukin 1α is a marker of endothelial cellular senescent. *Immun. Ageing* **3,** 4
4. Kumar, S., Millis, A. J., and Baglioni, C. (1992) Expression of interleukin 1-inducible genes and production of interleukin 1 by aging human fibroblasts. *Proc. Natl. Acad. Sci. U.S.A.* **89,** 4683–4687
5. Garfinkel, S., Brown, S., Wessendorf, J. H., and Maciag, T. (1994) Post-transcriptional regulation of interleukin 1α in various strains of young and senescent human umbilical vein endothelial cells. *Proc. Natl. Acad. Sci. U.S.A.* **91,** 1559–1563
6. Orjalo, A. V., Bhaumik, D., Gengler, B. K., Scott, G. K., and Campisi, J. (2009) Cell surface-bound IL-1α is an upstream regulator of the senescence-associated IL-6/IL-8 cytokine network. *Proc. Natl. Acad. Sci. U.S.A.* **106,** 17031–17036
7. Kobayashi, Y., Yamamoto, K., Saido, T., Kawasaki, H., Oppenheim, J. J., and Matsushima, K. (1990) Identification of calcium-activated neutral protease as a processing enzyme of human interleukin 1α. *Proc. Natl. Acad. Sci. U.S.A.* **87,** 5548–5552
8. Stevenson, F. T., Turck, J., Locksley, R. M., and Lovett, D. H. (1997) The N-terminal propiece of interleukin 1α is a transforming nuclear oncoprotein. *Proc. Natl. Acad. Sci. U.S.A.* **94,** 508–513
9. Werman, A., Werman-Venkert, R., White, R., Lee, J. K., Werman, B., Krelin, Y., Voronov, E., Dinarello, C. A., and Apte, R. N. (2004) The precursor form of IL-1α is an intracrine proinflammatory activator of transcription. *Proc. Natl. Acad. Sci. U.S.A.* **101,** 2434–2439
10. Afonina, I. S., Tynan, G. A., Logue, S. E., Cullen, S. P., Bots, M., Lüthi, A. U., Reeves, E. P., McElvaney, N. G., Medema, J. P., Lavelle, E. C., and Martin, S. J. (2011) Granzyme B-dependent proteolysis acts as a switch to enhance the proinflammatory activity of IL-1α. *Mol. Cell* **44,** 265–278
11. Dasgupta, J., Kar, S., Liu, R., Joseph, J., Kalyanaraman, B., Remington, S. J., Chen, C., and Melendez, J. A. (2010) Reactive oxygen species control senescence-associated matrix metalloproteinase-1 through c-Jun N-terminal kinase. *J. Cell. Physiol.* **225,** 52–62
12. Chen, Q., Fischer, A., Reagan, J. D., Yan, L. J., and Ames, B. N. (1995) Oxidative DNA damage and senescence of human diploid fibroblast cells. *Proc. Natl. Acad. Sci. U.S.A.* **92,** 4337–4341
13. Saito, H., Hammond, A. T., and Moses, R. E. (1995) The effect of low oxygen tension on the *in vitro*-replicative life span of human diploid fibroblast cells and their transformed derivatives. *Exp. Cell Res.* **217,** 272–279
14. Guikema, B. J., Ginnan, R., Singer, H. A., and Jourd'heuil, D. (2005) Catalase potentiates interleukin-1β-induced expression of nitric oxide synthase in rat vascular smooth muscle cells. *Free Radic. Biol. Med.* **38,** 597–605
15. Gleichmann, M., and Mattson, M. P. (2011) Neuronal calcium homeostasis and dysregulation. *Antioxid. Redox Signal.* **14,** 1261–1273
16. Galan, C., Jardín, I., Dionisio, N., Salido, G., and Rosado, J. A. (2010) Role of oxidant scavengers in the prevention of Ca^{2+} homeostasis disorders. *Molecules* **15,** 7167–7187
17. Trebak, M., Ginnan, R., Singer, H. A., and Jourd'heuil, D. (2010) Interplay between calcium and reactive oxygen/nitrogen species: an essential paradigm for vascular smooth muscle signaling. *Antioxid. Redox Signal.* **12,** 657–674
18. Badugu, R., Garcia, M., Bondada, V., Joshi, A., and Geddes, J. W. (2008) N terminus of calpain 1 is a mitochondrial targeting sequence. *J. Biol. Chem.* **283,** 3409–3417
19. Cohen, I., Rider, P., Carmi, Y., Braiman, A., Dotan, S., White, M. R., Voronov, E., Martin, M. U., Dinarello, C. A., and Apte, R. N. (2010) Differential release of chromatin-bound IL-1α discriminates between necrotic and apoptotic cell death by the ability to induce sterile inflammation. *Proc. Natl. Acad. Sci. U.S.A.* **107,** 2574–2579
20. Coppé, J. P., Patil, C. K., Rodier, F., Sun, Y., Muñoz, D. P., Goldstein, J., Nelson, P. S., Desprez, P. Y., and Campisi, J. (2008) Senescence-associated secretory phenotypes reveal cell-nonautonomous functions of oncogenic RAS and the p53 tumor suppressor. *PLoS Biol.* **6,** 2853–2868
21. Keely, P. J., Westwick, J. K., Whitehead, I. P., Der, C. J., and Parise, L. V. (1997) Cdc42 and Rac1 induce integrin-mediated cell motility and invasiveness through PI(3)K. *Nature* **390,** 632–636
22. Chander, H., Truesdell, P., Meens, J., and Craig, A. W. (2013) Transducer of Cdc42-dependent actin assembly promotes breast cancer invasion and metastasis. *Oncogene* **32,** 3080–3090
23. Bates, R. C., DeLeo, M. J., 3rd, and Mercurio, A. M. (2004) The epithelial-mesenchymal transition of colon carcinoma involves expression of IL-8 and CXCR-1-mediated chemotaxis. *Exp. Cell Res.* **299,** 315–324

24. Sullivan, N. J., Sasser, A. K., Axel, A. E., Vesuna, F., Raman, V., Ramirez, N., Oberyszyn, T. M., and Hall, B. M. (2009) Interleukin-6 induces an epithelial-mesenchymal transition phenotype in human breast cancer cells. *Oncogene* **28,** 2940–2947
25. Burdsal, C. A., Damsky, C. H., and Pedersen, R. A. (1993) The role of E-cadherin and integrins in mesoderm differentiation and migration at the mammalian primitive streak. *Development* **118,** 829–844
26. Kim, K., Lu, Z., and Hay, E. D. (2002) Direct evidence for a role of β-catenin/LEF-1 signaling pathway in induction of EMT. *Cell Biol. Int.* **26,** 463–476
27. Reichert, M., Müller, T., and Hunziker, W. (2000) The PDZ domains of zonula occludens-1 induce an epithelial to mesenchymal transition of Madin-Darby canine kidney I cells. Evidence for a role of β-catenin/Tcf/Lef signaling. *J. Biol. Chem.* **275,** 9492–9500
28. Liebner, S., Cattelino, A., Gallini, R., Rudini, N., Iurlaro, M., Piccolo, S., and Dejana, E. (2004) β-Catenin is required for endothelial-mesenchymal transformation during heart cushion development in the mouse. *J. Cell Biol.* **166,** 359–367
29. Yan, W., Cao, Q. J., Arenas, R. B., Bentley, B., and Shao, R. (2010) GATA3 inhibits breast cancer metastasis through the reversal of epithelial-mesenchymal transition. *J. Biol. Chem.* **285,** 14042–14051
30. Law, M. E., Corsino, P. E., Jahn, S. C., Davis, B. J., Chen, S., Patel, B., Pham, K., Lu, J., Sheppard, B., Nørgaard, P., Hong, J., Higgins, P., Kim, J. S., Luesch, H., and Law, B. K. (2013) Glucocorticoids and histone deacetylase inhibitors cooperate to block the invasiveness of basal-like breast cancer cells through novel mechanisms. *Oncogene* **32,** 1316–1329
31. Clevers, H. (2006) Wnt/β-catenin signaling in development and disease. *Cell* **127,** 469–480
32. Sánchez-Tilló, E., de Barrios, O., Siles, L., Cuatrecasas, M., Castells, A., and Postigo, A. (2011) β-Catenin/TCF4 complex induces the epithelial-to-mesenchymal transition (EMT)-activator ZEB1 to regulate tumor invasiveness. *Proc. Natl. Acad. Sci. U.S.A.* **108,** 19204–19209
33. Emami, K. H., Nguyen, C., Ma, H., Kim, D. H., Jeong, K. W., Eguchi, M., Moon, R. T., Teo, J. L., Oh, S. W., Kim, H. Y., Moon, S. H., Ha, J. R., and Kahn, M. (2004) A small molecule inhibitor of β-catenin/CREB-binding protein transcription. *Proc. Natl. Acad. Sci. U.S.A.* **101,** 12682–12687
34. Canino, C., Mori, F., Cambria, A., Diamantini, A., Germoni, S., Alessandrini, G., Borsellino, G., Galati, R., Battistini, L., Blandino, R., Facciolo, F., Citro, G., Strano, S., Muti, P., Blandino, G., and Cioce, M. (2012) SASP mediates chemoresistance and tumor-initiating-activity of mesothelioma cells. *Oncogene* **31,** 3148–3163
35. Dewamitta, S. R., Nomura, T., Kawamura, I., Hara, H., Tsuchiya, K., Kurenuma, T., Shen, Y., Daim, S., Yamamoto, T., Qu, H., Sakai, S., Xu, Y., and Mitsuyama, M. (2010) Listeriolysin O-dependent bacterial entry into the cytoplasm is required for calpain activation and interleukin-1α secretion in macrophages infected with *Listeria monocytogenes*. *Infect. Immun.* **78,** 1884–1894
36. Gross, O., Yazdi, A. S., Thomas, C. J., Masin, M., Heinz, L. X., Guarda, G., Quadroni, M., Drexler, S. K., and Tschopp, J. (2012) Inflammasome activators induce interleukin-1α secretion via distinct pathways with differential requirement for the protease function of caspase-1. *Immunity* **36,** 388–400
37. Ahn, J. K., Koh, E. M., Cha, H. S., Lee, Y. S., Kim, J., Bae, E. K., and Ahn, K. S. (2008) Role of hypoxia-inducible factor-1α in hypoxia-induced expressions of IL-8, MMP-1 and MMP-3 in rheumatoid fibroblast-like synoviocytes. *Rheumatology* **47,** 834–839
38. Kim, K. S., Rajagopal, V., Gonsalves, C., Johnson, C., and Kalra, V. K. (2006) A novel role of hypoxia-inducible factor in cobalt chloride- and hypoxia-mediated expression of IL-8 chemokine in human endothelial cells. *J. Immunol.* **177,** 7211–7224
39. Cane, G., Ginouvès, A., Marchetti, S., Buscà, R., Pouysségur, J., Berra, E., Hofman, P., and Vouret-Craviari, V. (2010) HIF-1α mediates the induction of IL-8 and VEGF expression on infection with Afa/Dr diffusely adhering *E. coli* and promotes EMT-like behaviour. *Cell. Microbiol.* **12,** 640–653
40. Genetos, D. C., Cheung, W. K., Decaris, M. L., and Leach, J. K. (2010) Oxygen tension modulates neurite outgrowth in PC12 cells through a mechanism involving HIF and VEGF. *J. Mol. Neurosci.* **40,** 360–366